





## Electrodeposited Nanostructured $\text{CoFe}_2\text{O}_4$ for Overall Water Splitting and Supercapacitor Applications

Volume 9 • Issue 2 | February 2019

Article

# Electrodeposited Nanostructured $\text{CoFe}_2\text{O}_4$ for Overall Water Splitting and Supercapacitor Applications

Chunyang Zhang <sup>1</sup>, Sanket Bhoiyate <sup>1</sup>, Chen Zhao <sup>1</sup>, Pawan K. Kahol <sup>2</sup>, Nikolaos Kostoglou <sup>3,\*</sup> , Christian Mitterer <sup>3</sup> , Steven J. Hinder <sup>4</sup>, Mark A. Baker <sup>4</sup>, Georgios Constantinides <sup>5</sup>, Kyriaki Polychronopoulou <sup>6,7</sup> , Claus Rebholz <sup>8</sup> and Ram K. Gupta <sup>1,\*</sup> 

<sup>1</sup> Department of Chemistry, Pittsburg State University, Pittsburg, KS 66762, USA;

c Zhang@gus.pittstate.edu (C.Z.); sanketbhoiyate931@gmail.com (S.B.); czhao@gus.pittstate.edu (C.Z.)

<sup>2</sup> Department of Physics, Pittsburg State University, Pittsburg, KS 66762, USA; pkahol@pittstate.edu

<sup>3</sup> Department of Materials Science, Montanuniversität Leoben, 8700 Leoben, Austria; christian.mitterer@unileoben.ac.at

<sup>4</sup> Department of Mechanical Engineering Sciences, University of Surrey, Guildford, Surrey GU2 7XH, UK; s.hinder@surrey.ac.uk (S.J.H.); m.baker@surrey.ac.uk (M.A.B.)

<sup>5</sup> Department of Mechanical Engineering and Materials Science and Engineering, Cyprus University of Technology, 3036 Lemesos, Cyprus; g.constantinides@cut.ac.cy

<sup>6</sup> Department of Mechanical Engineering, Khalifa University of Science and Technology, P.O. Box 127788 Abu Dhabi, UAE; kyriaki.polychrono@ku.ac.ae

<sup>7</sup> Center for Catalysis and Separation, Khalifa University of Science and Technology, P.O. Box 127788 Abu Dhabi, UAE

<sup>8</sup> Department of Mechanical and Manufacturing Engineering, University of Cyprus, 1678 Nicosia, Cyprus; claus@ucy.ac.cy

\* Correspondence: nikolaos.kostoglou@unileoben.ac.at (N.K.); rgupta@pittstate.edu (R.K.G.); Tel.: +1-620-235-4763 (R.K.G.)

Received: 20 January 2019; Accepted: 12 February 2019; Published: 13 February 2019



**Abstract:** To contribute to solving global energy problems, a multifunctional  $\text{CoFe}_2\text{O}_4$  spinel was synthesized and used as a catalyst for overall water splitting and as an electrode material for supercapacitors. The ultra-fast one-step electrodeposition of  $\text{CoFe}_2\text{O}_4$  over conducting substrates provides an economic pathway to high-performance energy devices. Electrodeposited  $\text{CoFe}_2\text{O}_4$  on Ni-foam showed a low overpotential of 270 mV and a Tafel slope of 31 mV/dec. The results indicated a higher conductivity for electrodeposited compared with dip-coated  $\text{CoFe}_2\text{O}_4$  with enhanced device performance. Moreover, bending and chronoamperometry studies suggest excellent durability of the catalytic electrode for long-term use. The energy storage behavior of  $\text{CoFe}_2\text{O}_4$  showed high specific capacitance of 768 F/g at a current density of 0.5 A/g and maintained about 80% retention after 10,000 cycles. These results demonstrate the competitiveness and multifunctional applicability of the  $\text{CoFe}_2\text{O}_4$  spinel to be used for energy generation and storage devices.

**Keywords:**  $\text{CoFe}_2\text{O}_4$ ; OER; HER; supercapacitor; overall water splitting

## 1. Introduction

According to the report presented by the International Renewable Energy Agency (IRENA), the Renewable Energy Policy Network for the 21st Century (REN21), and the International Energy Agency, transport is the second largest energy end-use sector, accounting for 29% of the total final energy consumption in the year 2015 [1]. About 96% of this energy comes from petroleum products, making it heavily reliant on fossil fuels. Several companies such as Tesla, Toyota, Nissan, Mercedes-Benz, Hyundai, Honda, and others have targeted their automotive market in the way that global dependence on petroleum

resources is reduced [2,3]. Thus, major research focuses on multifunctional materials for green energy applications to be used for electric motor and fuel cell vehicles.

Spinel has recently attracted considerable research attention for energy applications [4–6]. They represent a group of composite metals with such multifunctional capabilities, having a formula of  $AB_2O_4$  (A and B are metal ions) [7]. Mixed phase composition of transition metals into spinel structure provides advantageous electrical and catalytic properties required characteristics for energy conversion and storage [4–6]. Previously, electroactive materials such as structured carbons [8–14], transition metal oxides, and sulfides [15–18] have been studied for applications in batteries, supercapacitors, and fuel cells, as well as for water splitting. However, the lower activity of carbon-based materials, the inferior electronic conductivity of transition metal oxides, and the poor stability of transition metal sulfides limit their applicability for future energy devices [14,19–21]. Transition metal-based systems including oxides, hydroxides, or sulfides of cobalt and iron have been studied in the past few years for energy conversion or storage applications [22–27]. However, these materials show limited electrochemical performance. Various studies suggest that spinels of cobalt and iron provide better electronic conductivity, a higher population of active sites, and thus better electrochemical performance. For example, Kumbhar et al. synthesized spinel  $CoFe_2O_4$  nano-flakes on a stainless steel substrate by a simple chemical route using an alkaline bath containing  $Co^{2+}$  and  $Fe^{2+}$  ions for supercapacitor application [28]. An impedance test of spinel electrodes showed the low equivalent series resistance of about  $1.1 \Omega$ . Yu et al. reported a novel hierarchical Cu on a CoFe layered double hydroxide (LDH) core-shell nanostructured catalyst for oxygen and hydrogen evolution reaction [29]. The unique structure of LDH provides more active sites, leading to better catalytic performance. Another report suggests the use of iron–cobalt oxide nanosheets ( $Fe_xCo_y$ -ONSs) as a stable water oxidation catalyst [30]. Excellent oxygen evolution reaction (OER) activity was observed as a result of mass diffusion/transport of  $OH^-$  ions facilitated by ultrathin nanosheets, improved electronic conductivity, and adsorption of  $H_2O$  onto close  $Co^{3+}$  sites.

Several methods such as solvothermal, hydrothermal, chemical co-precipitation, and solution reduction reaction are reported for the synthesis of iron–cobalt oxide [30–35]. Most of the synthesized iron–cobalt oxide samples were powders, which are coated onto conductive substrates by dip-coating. The use of electrically insulating binders reduces the conductivity and thus affects the electronic activity of the material. Furthermore, the stability and flexibility of the electrodes are also compromised. However, direct electrodeposition of materials on conductive substrates could overcome this problem. For example, Lu et al. fabricated a hierarchically structured three-dimensional nickel-iron composite on Ni-foam for efficient oxygen evolution catalyst electrode using a one-step electrodeposition [36]. Higher conductivity and active surface area of the material over the electrode resulted in better electrochemical performance.

In this work,  $CoFe_2O_4$  was deposited on Ni-foam and carbonized cotton cloth using a facile electrodeposition method. The synthesized  $CoFe_2O_4$  on Ni-foam exhibited high electrocatalytic activity for OER and hydrogen evolution reaction (HER) with small overpotential. In addition, the  $CoFe_2O_4$  electrode showed high specific capacitance of 768 F/g at the current density of 0.5 A/g, maintaining stable performance with 80% retention up to 10,000 charge–discharge cycles. Our results suggest that electrodeposited  $CoFe_2O_4$  on Ni-foam could be used as a multifunctional material for both water splitting and supercapacitor applications.

## 2. Results and Discussion

X-ray diffraction (XRD) was used to study phase purity and crystallinity of the synthesized samples. Figure S1 shows the XRD patterns of  $CoFe_2O_4$ ,  $CoFe_2O_4$  ED@NF, and  $CoFe_2O_4$  ED@carbonized cotton cloth (CCC). The XRD pattern of  $CoFe_2O_4$  shows characteristic peaks of (111), (220), (311), (400), (422), (511), (440), and (533) planes, corresponding to the cubic structure of  $FeCo_2O_4$ . No peaks other than those stemming from  $CoFe_2O_4$  were observed, confirming phase purity of the synthesized  $CoFe_2O_4$ . The XRD patterns of  $CoFe_2O_4$  ED@NF and  $CoFe_2O_4$  ED@CCC do not show any

peaks attributable to  $\text{CoFe}_2\text{O}_4$ , indicating either the amorphous nature of the electrodeposited  $\text{CoFe}_2\text{O}_4$  layer or the lack of sufficient diffracted X-ray signal from the coating on the porous Ni-foam structure.

An X-ray photoelectron spectroscopy (XPS) wide scan of the  $\text{CoFe}_2\text{O}_4$  surface is presented in Figure S2. The Co 2p and O 1s peaks are given in Figure 1. Considering the Co 2p peak shape, this is very consistent with spectra of  $\text{Co}_3\text{O}_4$  standards given by Gu et al. [37] and Yang et al. [38], showing a  $2p_{3/2}$  peak binding energy of 779.9 eV and a broad plateau-like satellite structure to higher binding energies between the  $2p_{3/2}$  and  $2p_{1/2}$  peaks. Thus, this peak shape and satellite structure is representative of mixed  $\text{Co}^{2+}/\text{Co}^{3+}$  chemical states. Compared with the Co 2p spectrum for  $\text{CoFe}_2\text{O}_4$  given by Gu et al. [37] and Sagu et al. [39], the peak shape of the electrodeposited  $\text{CoFe}_2\text{O}_4$  shows a peak shape that is more consistent with that of  $\text{Co}_3\text{O}_4$ , and hence a 1:1 stoichiometric  $\text{Co}^{2+}/\text{Co}^{3+}$  fraction rather than the  $\text{Co}^{2+}$  rich compound observed in these other studies. However, it should be noted that quantification of the XPS spectra shows an enrichment of Co at the surface, indicating that the XPS spectra and outermost surface composition are not fully representative of the bulk material. The O 1s spectrum (Figure 1b) shows a peak at 530.1 eV corresponding to the metal oxide, with peaks at 531.6 and 532.7 eV corresponding to hydroxyl and adsorbed water species, respectively.

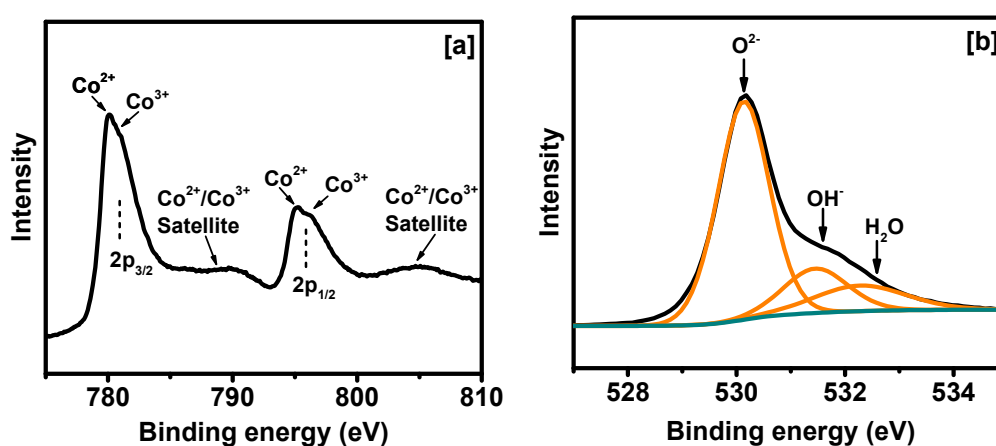
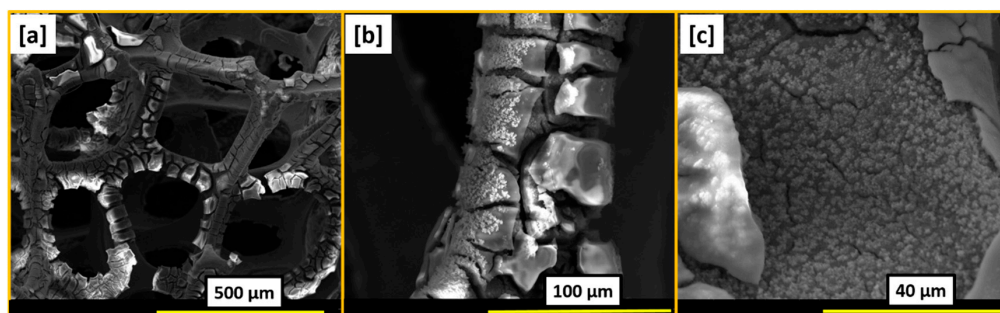


Figure 1. X-ray photoelectron spectroscopy (XPS) core level spectra of (a) Co 2p and (b) O 1s.

Figure 2a–c present scanning electron microscopy (SEM) images of electrodeposited  $\text{CoFe}_2\text{O}_4$  over Ni-foam at different magnifications. The coating over the Ni-foam is relatively uniform and dense, as observed from the images. The cracks in the coating are most likely the result of dehydration, associated with removal of the electrode from solution. The energy dispersive X-ray spectroscopy (EDS) O elemental image in Figure 3 confirms the general uniform distribution and composition of  $\text{CoFe}_2\text{O}_4$  over the Ni-foam substrate. However, the Fe and Co images in Figure 3 show that there are differences in the Fe/Co ratio between the ‘smoother’ surface regions and underlying ‘mottled’ areas of the coating. Considering the XPS results, it seems most likely that the smooth outer layer is  $\text{CoFe}_2\text{O}_4$  and this predominantly covers the Ni-foam. However, in some areas, this layer has become detached (possibly because of stresses associated with dehydration or transfer to the analytical laboratory), exposing a more Co-rich underlying layer. SEM images for  $\text{CoFe}_2\text{O}_4$  electrodeposited on CCC are given in Figure S3a–c, evidencing evenly coated fibers.

The OER activity of the  $\text{CoFe}_2\text{O}_4$  samples was studied by linear sweep voltammetry (LSV). The polarization curves for  $\text{CoFe}_2\text{O}_4$  ED@NF,  $\text{CoFe}_2\text{O}_4$ @NF, and  $\text{CoFe}_2\text{O}_4$  ED@CCC in 1M NaOH are shown in Figure 4a. The  $\text{CoFe}_2\text{O}_4$  ED@NF electrode required a low overpotential of 270 mV to achieve a current density of  $10 \text{ mA}/\text{cm}^2$ . This value is significantly lower than for  $\text{CoFe}_2\text{O}_4$ @NF (308 mV) and  $\text{CoFe}_2\text{O}_4$  ED@CCC (410 mV) electrodes. The observed difference could be the result of the high conductive pathway between the  $\text{CoFe}_2\text{O}_4$  catalyst and the Ni-foam, compared with the electrode synthesized by dip-coating. The Nyquist plot in Figure 4c at 0.5 V (versus SCE) shows lower charge transfer resistance for the  $\text{CoFe}_2\text{O}_4$  ED@NF electrode, which could be responsible for better catalytic

performance over other synthesized electrodes. The reduced impedance over increasing potential can be observed from the Nyquist plot for the  $\text{CoFe}_2\text{O}_4$  ED@NF electrode given in Figure S4. The kinetics of the OER reaction were analyzed using Tafel slopes (Figure 4b). The Tafel slope for  $\text{CoFe}_2\text{O}_4$  ED@NF,  $\text{CoFe}_2\text{O}_4$ @NF, and  $\text{CoFe}_2\text{O}_4$  ED@CCC was calculated to be 31, 47, and 119 mV/dec, respectively. The low Tafel slope value for the  $\text{CoFe}_2\text{O}_4$  ED@NF electrode indicates faster OER kinetics and can be correlated to the high electrocatalytic surface area of the electrodeposited Ni-foam electrode [15]. The electrochemical effective surface area was calculated using cyclic voltammetry (CV) curves in the non-faradic region (Figure S5) and the plotting relation of current density with respective scan rate is given in Figure 4d. A linear relationship was observed, showing a higher slope for  $\text{CoFe}_2\text{O}_4$  ED@NF ( $65 \text{ mC}/\text{cm}^2$ ) than  $\text{CoFe}_2\text{O}_4$ @NF ( $40 \text{ mC}/\text{cm}^2$ ) and  $\text{CoFe}_2\text{O}_4$  ED@CCC ( $3 \text{ mC}/\text{cm}^2$ ), thus indicating a larger effective electrochemical surface area. The higher surface area of  $\text{CoFe}_2\text{O}_4$  ED@NF is consistent with the excellent OER performance. The  $\text{CoFe}_2\text{O}_4$  ED@NF electrode of this study required a lower overpotential for achieving a current density of  $10 \text{ mA}/\text{cm}^2$  compared with other FeCo-based reports. For example, Yan et al. synthesized a  $\text{CoFe}_2\text{O}_4$  hybrid strongly coupled with carbon nanotubes and observed a higher overpotential ( $>0.6 \text{ V}$ ) to achieve  $5 \text{ mA}/\text{cm}^2$  in  $0.1 \text{ M KOH}$  [31]. Another hybrid of  $\text{CoFe}_2\text{O}_4$  nanoparticles supported on nitrogen/sulfur dual-doped three-dimensional (3D) reduced graphene oxide networks (CFO/NS-rGO) showed an overpotential of about  $0.55 \text{ V}$  to achieve the current density of  $10 \text{ mA}/\text{cm}^2$  [32]. The iron–cobalt oxide nanosheets (FeCo-ONS) prepared by Zhuang et al. required an overpotential of  $308 \text{ mV}$  to reach  $10 \text{ mA}/\text{cm}^2$  with a Tafel slope of  $36.8 \text{ mV}/\text{dec}$  [30]. Table S1 shows a detailed comparison of catalytic electrodes synthesized within this work with previously reported  $\text{CoFe}_2\text{O}_4$  samples. It can be observed that the  $\text{CoFe}_2\text{O}_4$  ED@NF electrode requires a low overpotential and shows higher kinetics of reaction compared with all the other reported values.



**Figure 2.** Scanning electron microscopy (SEM) images of electrodeposited  $\text{CoFe}_2\text{O}_4$  on Ni-foam.

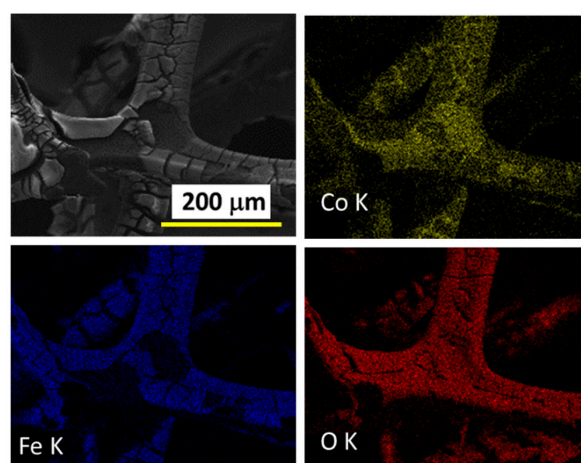


**Figure 3.** EDX elemental maps of electrodeposited  $\text{CoFe}_2\text{O}_4$  on Ni-foam revealing the distribution of Co, Fe, and O.

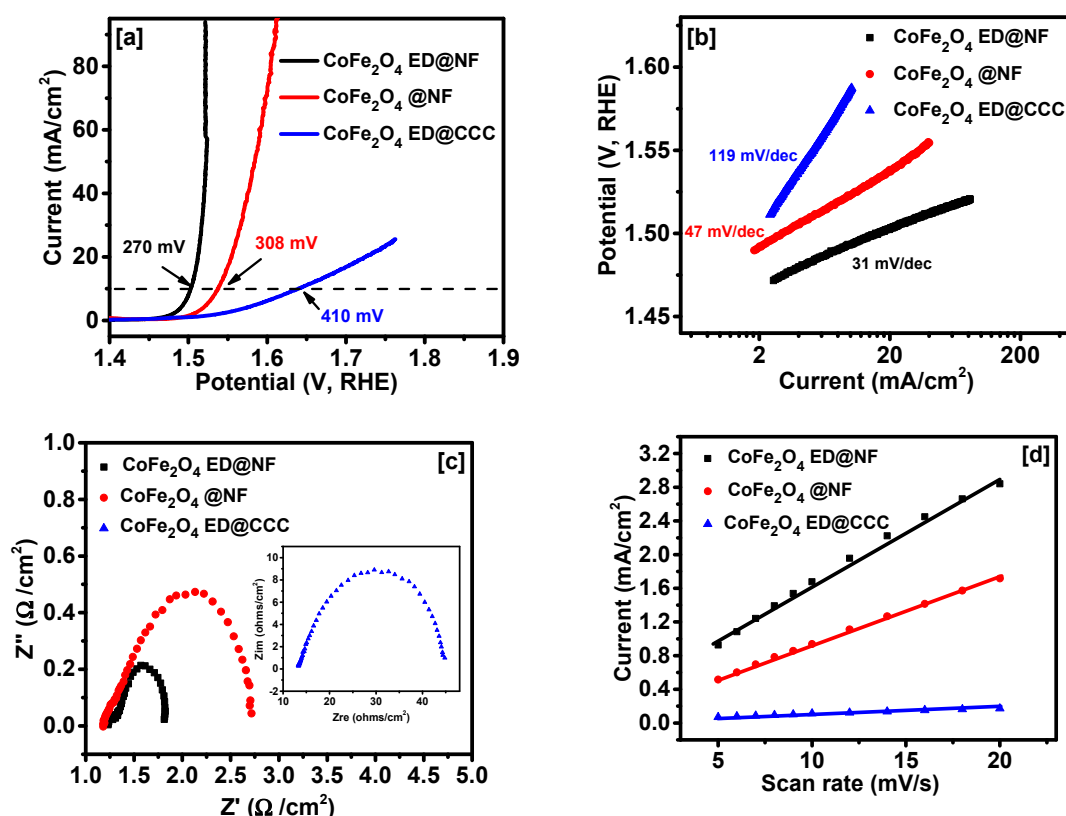


**Figure 4.** (a) Polarization curves, (b) Tafel slopes, (c) Nyquist plot at 0.5 V (vs. SCE), and (d) current density vs. scan rate plots for  $\text{CoFe}_2\text{O}_4$  electrodes. RHE—reversible hydrogen electrode; CCC—carbonized cotton cloth.

The effect of bending on the OER properties of the  $\text{CoFe}_2\text{O}_4$  ED@NF electrode was studied to investigate its potential to be used as a flexible electrode. The polarization curves in Figure 5a show almost identical behavior for curves before and after bending the electrode by a  $60^\circ$  angle. Moreover, the durability of the electrode was assessed for 17 h using chronoamperometry (Figure 5b). The chronical current measurement showed almost constant values without any detriment over the catalytic performance of the electrodes, suggesting the durable performance of the electrode for long-term use.

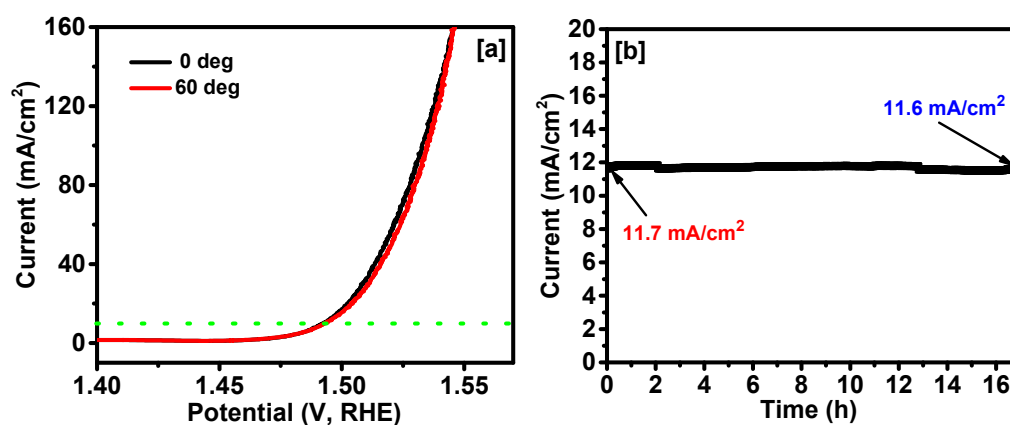


**Figure 5.** (a) Bending test and (b) chronoamperometry data for  $\text{CoFe}_2\text{O}_4$  ED@NF in oxygen evolution reaction (OER) range.

As several reports suggest the use of spinels for multifunctional catalytic application [7,31,40], herein we evaluated the performance of the  $\text{CoFe}_2\text{O}_4$  ED@NF electrode for HER catalysis. Figure S6a shows the LSV polarization curves. A small overpotential of  $-270$  mV was required to achieve the current density of  $-10$   $\text{mA}/\text{cm}^2$ . Moreover, the reaction kinetics using the Tafel slope yielded a low value of  $94$  mV/dec (Figure S6b). The value observed for the  $\text{CoFe}_2\text{O}_4$  electrode as HER catalyst was lower compared with other similar catalytic systems. For example, a hydrothermally synthesized  $\text{CoFe}_2\text{O}_4$  NPs-on-CFP electrode by Kargar and co-workers required an overpotential of  $-356$  mV to achieve a current of  $-10$   $\text{mA}/\text{cm}^2$  [41]. The comparison table of other reports based on Fe, Co, and other non-precious transition metals in alkaline media can be observed from Table S2. Moreover, the chronoamperometry test indicated a stable HER performance of the catalyst electrode for 17 h, suggesting long-term durability of the electrode (Figure S6c). This indicates that the  $\text{CoFe}_2\text{O}_4$  ED@NF electrode could be used as a bifunctional water-splitting catalyst.

An electrolyzer cell was fabricated using a two-electrode system to study water-splitting of catalytic electrodes. In this study, the  $\text{CoFe}_2\text{O}_4$  ED@NF electrode was used as an anode and a standard platinum carbon (Pt-C) electrode was used as a cathode. Figure 6a shows polarization curves using the LSV test for different electrolyzer cells. The  $\text{CoFe}_2\text{O}_4$ //Pt-C electrolyzer system required a low potential of  $1.56$  V to obtain a current density of  $10$   $\text{mA}/\text{cm}^2$  compared with benchmark electrolyzer cells such as  $\text{IrO}_2$ //Pt-C ( $1.57$  V),  $\text{IrO}_2$ // $\text{IrO}_2$  ( $1.77$  V), and Pt-C//Pt-C ( $1.64$  V), which all required higher potentials. Moreover, the chronoamperometry test yielded stable performance of the  $\text{CoFe}_2\text{O}_4$ //Pt-C electrolyzer system for more than 17 h, as evidenced by Figure 6b.

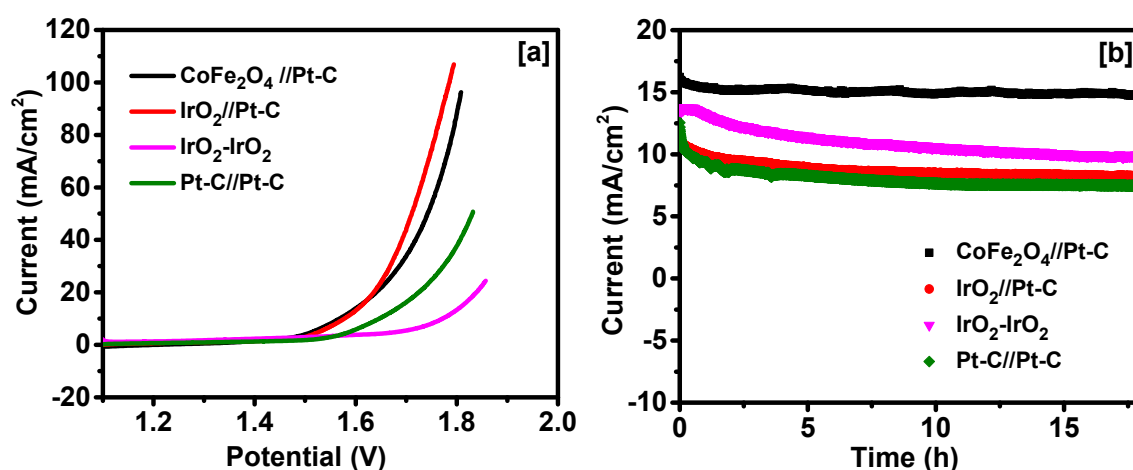


**Figure 6.** (a) Polarization and (b) chronoamperometry plots for overall water splitting of a two-electrode electrolyzer.

The energy storage capacity of the  $\text{CoFe}_2\text{O}_4$  ED@NF electrode was measured using CV. The specific capacitance values can be predicted based on the area under the CV curves. Figure 7a depicts the specific capacitance values as a function of varying scan rates. Higher specific capacitance values were observed with decreasing scan rates. A similar behavior was observed in other reports of energy storage systems [28,42–44]. The CV curves of  $\text{CoFe}_2\text{O}_4$  ED@NF in 3M KOH electrolyte at various scan rates are given in Figure S7a. Pairs of redox peaks in the CV curves indicate the pseudocapacitive behavior of the material. This resulted in a high specific capacitance of  $2246$  F/g at a scan rate of  $1$  mV/s. The charge storage behavior was further analyzed using the galvanostatic charge–discharge test. Figure 7b shows the relationship of specific capacitance at different current densities. At lower charging current, high capacitance values were obtained. A similar relation of current density with discharge time can be observed from Figure S7b. This could be the result of sufficient time provided for redox reactions at low current densities. Redox reactions promoted at low current densities lead to better charge storage compared with other non-faradic systems [43–46]. At a current density of  $0.5$  A/g,

a high specific capacitance of 768 F/g was observed. This result is comparable to other reported values for electrodes within an Co–Fe based system, as summarized in Table S3. Moreover, the stability test of the electrode showed high capacitance retention of about 80% after 10,000 cycles (Figure S8), which is better compared with other reports based on Co–Fe systems. For example, flower-like  $\text{CoFe}_2\text{O}_4/\text{FeOOH}$  nanocomposites maintain 91.3% retention after 1000 cycles [47]. For reduced graphene oxide– $\text{CoFe}_2\text{O}_4$  composites, the capacitance retention is about 78.1% after 1000 cycles [35]. This suggests that the synthesized  $\text{CoFe}_2\text{O}_4$  ED@NF electrodes showed higher charge storage capacities and stable performance to be used as energy storage electrode materials.

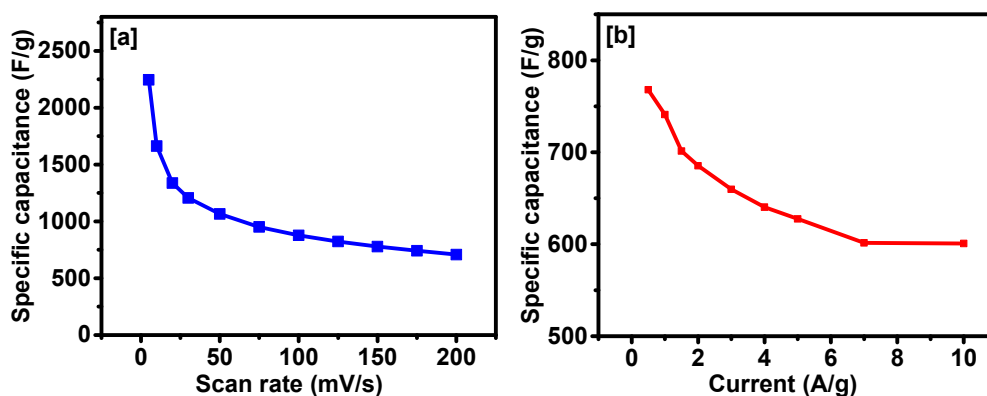


**Figure 7.** Variation of specific capacitance as a function of (a) scan rate and (b) current density for  $\text{FeCo}_2\text{O}_4$  ED @ Ni-foam.

### 3. Materials and Methods

#### 3.1. Materials

All chemicals were of analytical grade purity and were used without any further purification. Cobalt (II) nitrate and iron (III) nitrate (99.9%) were purchased from Sigma Aldrich, USA. All other chemicals were purchased from Fisher Scientific, USA.

#### 3.2. Preparation of Electrodeposited $\text{CoFe}_2\text{O}_4$ Electrodes

Nanostructured  $\text{CoFe}_2\text{O}_4$  was electrodeposited on Ni-foam and carbonized cotton cloth (CCC) using a standard three-electrode system. Before electrodeposition, Ni-foam was thoroughly cleaned [15]. In the three-electrode system, Ni-foam as a working electrode, a platinum plate as a counter electrode, and an Ag/AgCl electrode as a reference electrode were used. The electrolyte consists of an aqueous solution of 0.582 g of cobalt nitrate and 1.616 g of iron nitrate in 20 ml deionized water. The electrodeposition was carried out at  $-1.0$  V (vs. Ag/AgCl) for a period of 5 min to obtain a thin brown film covering the Ni-foam [48]. The average weight of the deposited material was  $1.2 \text{ mg/cm}^2$ .

Electrodeposition of  $\text{CoFe}_2\text{O}_4$  on the CCC was carried out using the above setup, where CCC was used instead of Ni-foam as a substrate. The CCC was prepared by calcination of carbon cloth in a tube furnace at  $800^\circ\text{C}$  for two hours under  $\text{N}_2$  atmosphere (at  $5^\circ\text{C}/\text{min}$ ) [49]. Electrodeposition of  $\text{CoFe}_2\text{O}_4$  on CCC was carried out under similar conditions, but for 50 min to achieve  $1.2 \text{ mg/cm}^2$  of the deposited material.

#### 3.3. Preparation of Dip-Coated $\text{CoFe}_2\text{O}_4$ Electrode

To compare the effect of the direct growth of  $\text{CoFe}_2\text{O}_4$  on a conducting surface, we have dip-coated  $\text{CoFe}_2\text{O}_4$  powders on the Ni-foam after synthesizing  $\text{CoFe}_2\text{O}_4$ . For this reason,  $\text{CoFe}_2\text{O}_4$  was synthesized by a simple hydrothermal method, where 0.582 g of cobalt nitrate, 1.616 g of iron nitrate, and 7.2 g of urea were dissolved in a mixture of 30 ml of isopropyl alcohol and 6 ml of water. The mixture was stirred for 30 min and transferred into a 45 mL Teflon-lined stainless-steel



autoclave. The reaction was carried out at 120 °C for 12 h. The resultant precipitates were washed several times using water and ethanol. The separation was carried out using centrifugation at 10,000 rpm, followed by drying under vacuum at 80 °C for 6 h and calcination at 350 °C in air for 2 h (5 °C/min). The CoFe<sub>2</sub>O<sub>4</sub> electrode was prepared by dipping the Ni-foam in a slurry of CoFe<sub>2</sub>O<sub>4</sub> powder (80 wt.%), acetylene black (10 wt.%), and polyvinylidene difluoride (10 wt.%) in N-methyl pyrrolidinone. The material loading on the Ni-foam was about 1.2 mg/cm<sup>2</sup>. Sample electrodes fabricated by deposition of CoFe<sub>2</sub>O<sub>4</sub> over Ni-foam using electrodeposition and dip-coating are termed in the following as CoFe<sub>2</sub>O<sub>4</sub> ED@NF and CoFe<sub>2</sub>O<sub>4</sub>@NF, respectively, while the sample electrodeposited over carbonized carbon cloth is referred to as CoFe<sub>2</sub>O<sub>4</sub> ED@CCC.

### 3.4. Characterization

The synthesized samples were characterized using various methods. X-ray diffraction (XRD) was used to study the crystallinity and phase purity of the samples. X-ray photoelectron spectroscopy (XPS) and scanning electron microscopy (SEM) equipped with energy dispersive X-ray spectroscopy (EDS) was used to investigate structural, chemical, and morphological properties. XRD patterns were recorded using a Shimadzu X-ray diffractometer (Lenexa, Kansas, USA). CuKα<sub>1</sub> radiation (λ = 1.5406 Å) in the 2θ-θ mode was used to study the crystallinity and phase purity of the synthesized samples. Microstructural properties of the samples were investigated using a Quanta 200 SEM (FEI, Hillsboro, Oregon, USA). The elemental compositions and elemental mapping of the synthesized samples were recorded for the synthesized samples using EDS. The chemical composition of the synthesized samples was determined using XPS analysis using a ThermoFisher Scientific Instruments (East Grinstead, UK). A monochromated Al Kα radiation source (hν = 1486.6 eV) and an X-ray spot of ~400 μm in radius were used for data recording. The elemental survey spectra were recorded using a pass energy of 200 eV. A passing energy of 50 eV was used for recording high-resolution core level spectra for all the elements. The Advantage software was used for the peak fittings.

Electrochemical performance was studied using a standard three-electrode system and a Versastat4-500 electrochemical workstation (Princeton Applied Research, TN, USA). CoFe<sub>2</sub>O<sub>4</sub> electrodes were used as working electrodes. Cyclic voltammetry (CV), galvanostatic charge-discharge (GCD), and electrochemical impedance spectroscopy (EIS) measurements were performed to examine the energy storage performance of electrodes in 3M KOH electrolyte. The electrocatalytic behavior of the CoFe<sub>2</sub>O<sub>4</sub> electrodes for OER and HER was measured in 1M NaOH electrolyte. Electrocatalytic testing includes linear sweep voltammetry (LSV), cyclic voltammetry (CV), chronoamperometry, and electrochemical impedance spectroscopy (EIS). LSV was performed at a scan rate of 1 mV/s in both the OER and HER region. The potential was converted to a reversible hydrogen electrode (RHE) using the Nernst equation. All the EIS measurements were recorded in a frequency range of 0.05 Hz to 10 kHz with an applied 10 mV of AC amplitude.

## 4. Conclusions

In summary, we synthesized an efficient catalyst and energy storage material using a facile, ultra-fast, and one-step electrodeposition method to grow CoFe<sub>2</sub>O<sub>4</sub> over Ni-foam and carbon cloth. A uniform distribution of CoFe<sub>2</sub>O<sub>4</sub> electrochemically deposited over the surface of the substrate was observed through SEM and EDX. A low overpotential of 270 mV was calculated for OER when CoFe<sub>2</sub>O<sub>4</sub> was grown over Ni-foam using electrodeposition. The obtained low Tafel slope of 31 mV/dec compared with a dip-coated sample represents excellent reaction kinetics. This could be attributed to a high conductive pathway stemming from the CoFe<sub>2</sub>O<sub>4</sub> deposited over Ni-foam. Flexibility and chronoamperometry evidenced the stable catalytic performance of the electrodes. The energy storage capacity of the material using galvanostatic charge-discharge test show high specific capacitance of 768 F/g at a current density of 0.5 A/g. Stability of electrodes after 10,000 cycles showed capacitance retention of 80%. The obtained results reveal the promising potential of efficient, multi-functional, and cost-effective CoFe<sub>2</sub>O<sub>4</sub> catalysts for energy generation and storage systems.

**Supplementary Materials:** The following are available online at <http://www.mdpi.com/2073-4344/9/2/176/s1>, Figure S1. XRD patterns of (a) CoFe<sub>2</sub>O<sub>4</sub>, (b) CoFe<sub>2</sub>O<sub>4</sub> ED@CCC and CoFe<sub>2</sub>O<sub>4</sub> ED@NF. Figure S2. XPS wide scan of the CoFe<sub>2</sub>O<sub>4</sub>. Figure S3. SEM images of electrodeposited CoFe<sub>2</sub>O<sub>4</sub> on carbonized carbon cloth. Figure S4. Nyquist plots for the CoFe<sub>2</sub>O<sub>4</sub> ED@NF sample at various potentials (vs. SCE). Figure S5. CV curves in non-faradic region for (a) CoFe<sub>2</sub>O<sub>4</sub> ED@NF, (b) CoFe<sub>2</sub>O<sub>4</sub>@NF, and (c) CoFe<sub>2</sub>O<sub>4</sub> ED@CCC. Figure S6. (a): Polarization curves, (b) Tafel slopes, and (c) chronoamperometry data for CoFe<sub>2</sub>O<sub>4</sub> ED@NF in HER range. Figure S7. (a) CV curves and (b) GCD curves of CoFe<sub>2</sub>O<sub>4</sub> ED@NF obtained at various scan rates and current densities in 3M KOH electrolyte. Figure S8. Cyclic stability plot for CoFe<sub>2</sub>O<sub>4</sub> ED@NF sample using 10,000 galvanostatic charge-discharge measurements. Table S1. Comparison of OER performance of some recently reported FeCo-based electrocatalysts. Table S2. Comparison of HER performance of some recently reported electrocatalysts in alkaline media. Table S3. Comparison of specific capacitances of some reported FeCo-based samples.

**Author Contributions:** R.K.G. conceived the project, designed the experiments, interpreted the data, and finalized the manuscript. The first draft of the manuscript was written by C.Z. (Chunyang Zhang) and S.B. C.Z. (Chunyang Zhang) and S.B. performed all the electrochemical measurements and recorded the X.R.D. data. G.C. provided SEM/EDS images and analysis. M.B. and S.H. provided X.P.S. data and analysis. All authors reviewed and commented on the manuscript.

**Funding:** This research received no external funding. The APC was funded by the Abu Dhabi Education and Knowledge (ADEK) Department, Award for Research Excellence, AARE 2017.

**Acknowledgments:** Ram K. Gupta expresses his sincere acknowledgment to the Polymer Chemistry Program and the Kansas Polymer Research Center, Pittsburg State University, for providing financial and research support to complete this project.

**Conflicts of Interest:** The authors declare no conflict of interest.

## References

1. IRENA; IEA; REN21. *Renewable Energy Policies in a Time of Transition*. 2018. Available online: <https://www.irena.org/publications/2018/Apr/Renewable-energy-policies-in-a-time-of-transition>.
2. Mitch Jacoby. Fuel-Cell Cars Finally Drive off the Lot. *Chem. Eng. News Arch.* **2017**, *95*, 28.
3. Rissman, J. The Future Of Electric Vehicles In The U.S., Part 1: 65%-75% New Light-Duty Vehicle Sales By 2050. *Forbes*, 14 September 2017; 1.
4. Hu, H.; Guan, B.; Xia, B.; Lou, X.W. Designed Formation of Co<sub>3</sub>O<sub>4</sub>/NiCo<sub>2</sub>O<sub>4</sub> Double-Shelled Nanocages with Enhanced Pseudocapacitive and Electrocatalytic Properties. *J. Am. Chem. Soc.* **2015**, *137*, 5590–5595. [[CrossRef](#)] [[PubMed](#)]
5. Fu, W.; Zhao, C.; Han, W.; Liu, Y.; Zhao, H.; Ma, Y.; Xie, E. Cobalt Sulfide Nanosheets Coated on NiCo<sub>2</sub>S<sub>4</sub> Nanotube Arrays as Electrode Materials for High-Performance Supercapacitors. *J. Mater. Chem. A* **2015**, *3*, 10492–10497. [[CrossRef](#)]
6. Chauhan, M.; Reddy, K.P.; Gopinath, C.S.; Deka, S. Copper Cobalt Sulfide Nanosheets Realizing a Promising Electrocatalytic Oxygen Evolution Reaction. *ACS Catal.* **2017**, *7*, 5871–5879. [[CrossRef](#)]
7. Zhao, Q.; Yan, Z.; Chen, C.; Chen, J. Spinels: Controlled Preparation, Oxygen Reduction/Evolution Reaction Application, and Beyond. *Chem. Rev.* **2017**, *117*, 10121–10211. [[CrossRef](#)] [[PubMed](#)]
8. Kostoglou, N.; Koczwara, C.; Prehal, C.; Terziyska, V.; Babic, B.; Matovic, B.; Constantinides, G.; Tampaxis, C.; Charalambopoulou, G.; Steriotis, T.; et al. Nanoporous Activated Carbon Cloth as a Versatile Material for Hydrogen Adsorption, Selective Gas Separation and Electrochemical Energy Storage. *Nano Energy* **2017**, *40*, 49–64. [[CrossRef](#)]
9. Talapaneni, S.N.; Lee, J.H.; Je, S.H.; Buyukcakir, O.; Kwon, T.; Polychronopoulou, K.; Choi, J.W.; Coskun, A. Chemical Blowing Approach for Ultramicroporous Carbon Nitride Frameworks and Their Applications in Gas and Energy Storage. *Adv. Funct. Mater.* **2017**, *27*, 1604658. [[CrossRef](#)]
10. Li, Y.; Samad, Y.A.; Polychronopoulou, K.; Alhassan, S.M.; Liao, K. From Biomass to High Performance Solar-thermal and Electric-thermal Energy Conversion and Storage Materials. *J. Mater. Chem. A* **2014**, *2*, 7759–7765. [[CrossRef](#)]
11. Chen, S.; Bi, J.; Zhao, Y.; Yang, L.; Zhang, C.; Ma, Y.; Wu, Q.; Wang, X.; Hu, Z. Nitrogen-Doped Carbon Nanocages as Efficient Metal-Free Electrocatalysts for Oxygen Reduction Reaction. *Adv. Mater.* **2012**, *24*, 5593–5597. [[CrossRef](#)]
12. Balogun, M.-S.; Qiu, W.; Yang, H.; Fan, W.; Huang, Y.; Fang, P.; Li, G.; Ji, H.; Tong, Y. A Monolithic Metal-Free Electrocatalyst for Oxygen Evolution Reaction and Overall Water Splitting. *Energy Environ. Sci.* **2016**, *9*, 3411–3416. [[CrossRef](#)]

13. Li, W.; Liang, C.; Qiu, J.; Zhou, W.; Han, H.; Wei, Z.; Sun, G.; Xin, Q. Carbon Nanotubes as Support for Cathode Catalyst of a Direct Methanol Fuel Cell. *Carbon N. Y.* **2002**, *40*, 791–794. [[CrossRef](#)]
14. Zheng, Y.; Liu, J.; Liang, J.; Jaroniec, M.; Qiao, S.Z. Graphitic Carbon Nitride Materials: Controllable Synthesis and Applications in Fuel Cells and Photocatalysis. *Energy Environ. Sci.* **2012**, *5*, 6717–6731. [[CrossRef](#)]
15. Ranaweera, C.K.; Zhang, C.; Bhoyate, S.; Kahol, P.K.; Ghimire, M.; Mishra, S.R.; Perez, F.; Gupta, B.K.; Gupta, R.K. Flower-Shaped Cobalt Oxide Nano-Structures as an Efficient, Flexible and Stable Electrocatalyst for the Oxygen Evolution Reaction. *Mater. Chem. Front.* **2017**, *1*, 1580–1584. [[CrossRef](#)]
16. Chen, J.; Xu, L.; Li, W.; Gou, X. Fe<sub>2</sub>O<sub>3</sub> Nanotubes in Gas Sensor and Lithium-Ion Battery Applications. *Adv. Mater.* **2005**, *17*, 582–586. [[CrossRef](#)]
17. Zhang, C.; Wang, Z.; Bhoyate, S.; Morey, T.; Neria, B.L.; Vasiraju, V.; Gupta, G.; Palchoudhury, S.; Kahol, P.K.; Mishra, S.R.; et al. MoS<sub>2</sub> Decorated Carbon Nanofibers as Efficient and Durable Electrocatalyst for Hydrogen Evolution Reaction. *C* **2017**, *3*, 33. [[CrossRef](#)]
18. Shi, J.; Li, X.; He, G.; Zhang, L.; Li, M. Electrodeposition of High-Capacitance 3D CoS/Graphene Nanosheets on Nickel Foam for High-Performance Aqueous Asymmetric Supercapacitors. *J. Mater. Chem. A* **2015**, *3*, 20619–20626. [[CrossRef](#)]
19. Joo, S.H.; Choi, S.J.; Oh, I.; Kwak, J.; Liu, Z.; Terasaki, O.; Ryoo, R. Ordered Nanoporous Arrays of Carbon Supporting High Dispersions of Platinum Nanoparticles. *Nature* **2001**, *412*, 169–172. [[CrossRef](#)] [[PubMed](#)]
20. Transition-metal-oxide, B.; Carbon, N.S.; Chen, P.; Shen, G.; Shi, Y.; Chen, H.; Zhou, C. Preparation and Characterization of Flexible Asymmetric Supercapacitors. *ACS Nano* **2010**, *4*, 4403–4411.
21. Shen, L.; Wang, J.; Xu, G.; Li, H.; Dou, H.; Zhang, X. NiCo<sub>2</sub>S<sub>4</sub> Nanosheets Grown on Nitrogen-Doped Carbon Foams as an Advanced Electrode for Supercapacitors. *Adv. Energy Mater.* **2015**, *5*, 2–8. [[CrossRef](#)]
22. Zaquine, C.; Bhoyate, S.; Wang, F.; Li, X.; Siam, K.; Kahol, P.K.; Gupta, R.K. Effect of Solvent for Tailoring the Nanomorphology of Multinary CuCo<sub>2</sub>S<sub>4</sub> for Overall Water Splitting and Energy Storage. *J. Alloys Compd.* **2019**, *784*, 1–7. [[CrossRef](#)]
23. Liu, R.; Jiang, Z.; Liu, Q.; Zhu, X.; Liu, L.; Ni, L.; Shen, C. Novel Red Blood Cell Shaped  $\alpha$ -Fe<sub>2</sub>O<sub>3</sub> Microstructures and FeO(OH) Nanorods as High Capacity Supercapacitors. *RSC Adv.* **2015**, *5*, 91127–91133. [[CrossRef](#)]
24. Guan, C.; Liu, J.; Wang, Y.; Mao, L.; Fan, Z.; Shen, Z.; Zhang, H.; Wang, J. Iron Oxide-Decorated Carbon for Supercapacitor Anodes with Ultrahigh Energy Density and Outstanding Cycling Stability. *ACS Nano* **2015**, *9*, 5198–5207. [[CrossRef](#)] [[PubMed](#)]
25. Lorkit, P.; Panapoy, M.; Ksapabutr, B. Iron Oxide-Based Supercapacitor from Ferratranne Precursor via Sol-gel-Hydrothermal Process. *Energy Procedia* **2014**, *56*, 466–473. [[CrossRef](#)]
26. Liu, J.; Nai, J.; You, T.; An, P.; Zhang, J.; Ma, G.; Niu, X.; Liang, C.; Yang, S.; Guo, L. The Flexibility of an Amorphous Cobalt Hydroxide Nanomaterial Promotes the Electrocatalysis of Oxygen Evolution Reaction. *Small* **2018**, *14*, 1703514. [[CrossRef](#)] [[PubMed](#)]
27. Numan, A.; Duraisamy, N.; Saiha Omar, F.; Mahipal, Y.K.; Ramesh, K.; Ramesh, S. Enhanced Electrochemical Performance of Cobalt Oxide Nanocube Intercalated Reduced Graphene Oxide for Supercapacitor Application. *RSC Adv.* **2016**, *6*, 34894–34902. [[CrossRef](#)]
28. Kumbhar, V.S.; Jagadale, A.D.; Shinde, N.M.; Lokhande, C.D. Chemical Synthesis of Spinel Cobalt Ferrite (CoFe<sub>2</sub>O<sub>4</sub>) Nano-Flakes for Supercapacitor Application. *Appl. Surf. Sci.* **2012**, *259*, 39–43. [[CrossRef](#)]
29. Yu, L.; Zhou, H.; Sun, J.; Qin, F.; Luo, D.; Xie, L.; Yu, F.; Bao, J.; Li, Y.; Yu, Y.; Chen, S.; Ren, Z. Hierarchical Cu@CoFe Layered Double Hydroxide Core-Shell Nanoarchitectures as Bifunctional Electrocatalysts for Efficient Overall Water Splitting. *Nano Energy* **2017**, *41*, 327–336. [[CrossRef](#)]
30. Zhuang, L.; Ge, L.; Yang, Y.; Li, M.; Jia, Y.; Yao, X.; Zhu, Z. Ultrathin Iron-Cobalt Oxide Nanosheets with Abundant Oxygen Vacancies for the Oxygen Evolution Reaction. *Adv. Mater.* **2017**, *29*, 1606793–1–1606793-7. [[CrossRef](#)]
31. Yan, W.; Bian, W.; Jin, C.; Tian, J.H.; Yang, R. An Efficient Bi-Functional Electrocatalyst Based on Strongly Coupled CoFe<sub>2</sub>O<sub>4</sub>/Carbon Nanotubes Hybrid for Oxygen Reduction and Oxygen Evolution. *Electrochim. Acta* **2015**, *177*, 65–72. [[CrossRef](#)]
32. Yan, W.; Cao, X.; Tian, J.; Jin, C.; Ke, K.; Yang, R. Nitrogen/Sulfur Dual-Doped 3D Reduced Graphene Oxide Networks-Supported CoFe<sub>2</sub>O<sub>4</sub> with Enhanced Electrocatalytic Activities for Oxygen Reduction and Evolution Reactions. *Carbon N. Y.* **2016**, *99*, 195–202. [[CrossRef](#)]

33. Lee, S.; Kang, J.S.; Leung, K.T.; Lee, W.; Kim, D.; Han, S.; Yoo, W.; Yoon, H.J.; Nam, K.; Sohn, Y. Unique Multi-Phase Co/Fe/CoFe<sub>2</sub>O<sub>4</sub> by Water–gas Shift Reaction, CO Oxidation and Enhanced Supercapacitor Performances. *J. Ind. Eng. Chem.* **2016**, *43*, 69–77. [[CrossRef](#)]
34. Lv, L.; Xu, Q.; Ding, R.; Qi, L.; Wang, H. Chemical Synthesis of Mesoporous CoFe<sub>2</sub>O<sub>4</sub> Nanoparticles as Promising Bifunctional Electrode Materials for Supercapacitors. *Mater. Lett.* **2013**, *111*, 35–38. [[CrossRef](#)]
35. He, P.; Yang, K.; Wang, W.; Dong, F.; Du, L.; Deng, Y. Reduced Graphene Oxide-CoFe<sub>2</sub>O<sub>4</sub> Composites for Supercapacitor Electrode. *Russ. J. Electrochem.* **2013**, *49*, 359–364. [[CrossRef](#)]
36. Lu, X.; Zhao, C. Electrodeposition of Hierarchically Structured Three-Dimensional Nickel–iron Electrodes for Efficient Oxygen Evolution at High Current Densities. *Nat. Commun.* **2015**, *6*, 6616. [[CrossRef](#)]
37. Gu, D.; Jia, C.-J.; Weidenthaler, C.; Bongard, H.-J.; Spliethoff, B.; Schmidt, W.; Schüth, F. Highly Ordered Mesoporous Cobalt-Containing Oxides: Structure, Catalytic Properties, and Active Sites in Oxidation of Carbon Monoxide. *J. Am. Chem. Soc.* **2015**, *137*, 11407–11418. [[CrossRef](#)]
38. Yang, J.; Liu, H.; Martens, W.N.; Frost, R.L. Synthesis and Characterization of Cobalt Hydroxide, Cobalt Oxyhydroxide, and Cobalt Oxide Nanodiscs. *J. Phys. Chem. C* **2010**, *114*, 111–119. [[CrossRef](#)]
39. Sagu, J.S.; Wijayantha, K.G.U.; Tahir, A.A. The Pseudocapacitive Nature of CoFe<sub>2</sub>O<sub>4</sub> Thin Films. *Electrochim. Acta* **2017**, *246*, 870–878. [[CrossRef](#)]
40. Yuan, C.; Wu, H.B.; Xie, Y.; Lou, X.W.D. Mixed Transition-Metal Oxides: Design, Synthesis, and Energy-Related Applications. *Angew. Chemie Int. Ed.* **2014**, *53*, 1488–1504. [[CrossRef](#)]
41. Kargar, A.; Yavuz, S.; Kim, T.K.; Liu, C.H.; Kuru, C.; Rustomji, C.S.; Jin, S.; Bandaru, P.R. Solution-Processed CoFe<sub>2</sub>O<sub>4</sub> Nanoparticles on 3D Carbon Fiber Papers for Durable Oxygen Evolution Reaction. *ACS Appl. Mater. Interfaces* **2015**, *7*, 17851–17856. [[CrossRef](#)] [[PubMed](#)]
42. Shanmugavani, A.; Kalpana, D.; Selvan, R.K. Electrochemical Properties of CoFe<sub>2</sub>O<sub>4</sub> Nanoparticles as Negative and Co(OH)<sub>2</sub> and Co<sub>2</sub>Fe(CN)<sub>6</sub> as Positive Electrodes for Supercapacitors. *Mater. Res. Bull.* **2015**, *71*, 133–141. [[CrossRef](#)]
43. Bhoyate, S.; Kahol, P.K.; Sapkota, B.; Mishra, S.R.; Perez, F.; Gupta, R.K. Polystyrene Activated Linear Tube Carbon Nanofiber for Durable and High-Performance Supercapacitors. *Surf. Coatings Technol.* **2018**, *345*, 113–122. [[CrossRef](#)]
44. Bhoyate, S.; Ranaweera, C.K.; Zhang, C.; Morey, T.; Hyatt, M.; Kahol, P.K.; Ghimire, M.; Mishra, S.R.; Gupta, R.K. Eco-Friendly and High Performance Supercapacitors for Elevated Temperature Applications Using Recycled Tea Leaves. *Glob. Challenges* **2017**, *1*, 1700063. [[CrossRef](#)]
45. Bhoyate, S.; Mensah-Darkwa, K.; Kahol, P.K.; Gupta, R.K. Recent Development on Nanocomposites of Graphene for Supercapacitor Applications. *Curr. Graphene Sci.* **2017**, *1*, 26–43. [[CrossRef](#)]
46. Adhikari, H.; Ghimire, M.; Ranaweera, C.K.; Bhoyate, S.; Gupta, R.K.; Alam, J.; Mishra, S.R. Synthesis and Electrochemical Performance of Hydrothermally Synthesized Co<sub>3</sub>O<sub>4</sub> Nanostructured Particles in Presence of Urea. *J. Alloys Compd.* **2017**, *708*, 628–638. [[CrossRef](#)]
47. Zhang, Y.X.; Hao, X.D.; Diao, Z.P.; Li, J.; Guan, Y.M. One-Pot Controllable Synthesis of Flower-like CoFe<sub>2</sub>O<sub>4</sub>/FeOOH Nanocomposites for High-Performance Supercapacitors. *Mater. Lett.* **2014**, *123*, 229–234. [[CrossRef](#)]
48. Zhang, C.; Bhoyate, S.; Kahol, P.K.; Siam, K.; Poudel, T.P.; Mishra, S.R.; Perez, F.; Gupta, A.; Gupta, G.; Gupta, R.K. Highly Efficient and Durable Electrocatalyst based on Nanowires of Cobalt Sulfide for Overall Water Splitting. *Chem. Nano Mat.* **2018**, *4*, 1240–1246. [[CrossRef](#)]
49. Zhang, C.; Bhoyate, S.; Hyatt, M.; Neria, B.L.; Siam, K.; Kahol, P.K.; Ghimire, M.; Mishra, S.R.; Perez, F.; Gupta, R.K. Nitrogen-Doped Flexible Carbon Cloth for Durable Metal Free Electrocatalyst for Overall Water Splitting. *Surf. Coatings Technol.* **2018**, *347*, 407–413. [[CrossRef](#)]

